Structural Design and Modelling of the Zigzag Wingbox for Span Morphing Wing

R.M. Ajaj[1], E.I. Saavedra Flores[1], MI. Friswell[1], B.K.S. Woods[1], W.G. Dettmer[1], G. Allegri[2], and A.T. Isikveren[3]

[1]College of Engineering, Swansea University, Swansea, SA2 8PP, UK
[2]Department of Aerospace Engineering, University of Bristol, Bristol, BS8 1TR, UK
[3]Bauhaus Luftfahrt e.V., Lyonel-Feininger-Str. 28, Munich, 80807, Germany

This paper presents the Zigzag wingbox concept that allows the wing span to be varied. The wingbox consists of a rigid part and a morphing part. The rigid part is a semi-monocoque construction that houses the fuel tank. The morphing part consists of various morphing partitions where in each partition there are two spars each consisting of two C-beams hinged together. Each morphing partition is bounded by two ribs through which the spars are connected. The ribs transfer the loads between the spars of adjacent morphing partition and serves as the main structure to which the flexible skins are to be attached. The Zigzag wingbox concept is to be incorporated on a medium altitude long endurance (MALE) UAV to enhance operational performance and provide roll control. Equivalent modelling and preliminary sizing of the concept are performed to assess its feasibility and quantify its potential benefits.

I. Introduction

Continuous demands to enhance flight performance and control authority have focused the interest of aircraft designers on span morphing. Wings with large spans have good range and fuel efficiency, but lack manoeuvrability and have relatively low cruise speeds. By contrast, aircraft with low aspect ratio wings can fly faster and become more manoeuvrable, but show poor aerodynamic efficiency [1]. A variable span wing can potentially integrate into a single aircraft the advantages of both designs, making this emerging technology especially attractive for military UAVs. Increasing the wingspan, increases the aspect ratio and wing area, and decreases the spanwise lift distribution for the same lift. Thus, the drag of the wing could be decreased, and consequently, the range or endurance of the vehicle increase. Unfortunately, the wing-root bending moment can increase considerably due to the larger span. Thus the aerodynamic, structural, aeroelastic, and control characteristics of the vehicle should be investigated in the design of variable-span morphing wings. Most span morphing concepts are based on a telescopic mechanism, following the ideas of Ivan Makhonine, a Russian expatriate, where the wing outer panel telescoped inside the inner panel to enable span and wing area changes. The MAK-10 was the first design with a telescopic wing and it first flew in 1931. The mechanism was powered pneumatically and enabled span increases up to 62% (from 13 to 21m) and area increases up to 57% (from 21 to 33m^2) [2]. Blondeau et al. [3] designed and fabricated a three segmented telescopic wing for a UAV. Hollow fiberglass shells were used to preserve the spanwise aerofoil geometry and ensure compact storage and deployment of the telescopic wing. To reduce the weight, they replaced the wing spars with inflatable actuators that could support the aerodynamic loads on the wing (in excess of 73kg/m^2). Their telescopic spar design consisted of three concentric circular aluminium tubes of decreasing diameter and increasing length, connected by ceramic linear bearings, and deployed and retracted using input pressures of 345–483kPa (50–70psi). The wing could undergo a 114% change in the aspect ratio, while supporting aerodynamic loads.

Blondeau et al. [4] adopted two identical telescopic spars instead of one, mechanically coupled by the ribs, to prevent wing twist and fluttering. The new prototype could undergo a 230% change in aspect ratio, and seam heights were reduced giving less parasitic drag. In its fully deployed condition the telescopic wing could achieve lift-to-drag ratios as high as 16, which was similar to its solid foam-core wing counterpart. The most dramatic morphing wing involving span change that has been realized as a wind tunnel prototype is the Agile Hunter by Lockheed Martin [5-7]. Funded by DARPA within the MAS program, the prototype was based on a military UAV capable of folding the inner sections of the wing near to the fuselage, to reduce the surface area and drag during transonic flight at low altitude (also called a Z-wing). The major challenge was the realization of suitable hinges that connect the two wing portions; the hinges have to sustain the aerodynamic loads but offer a smooth, continuous aerodynamic surface. Several materials were considered, including silicone-based and Shape Memory Polymer skins. Wind tunnel tests at Mach 0.6 showed a morphing capability from 0° to 130° over 65s with a controllable, reliable and precise actuation.

Asymmetrical span morphing can be used for roll control. Ajaj et al. [8] investigated the use of asymmetric span morphing to replace conventional ailerons and provide roll control for a medium altitude long endurance (MALE) UAV. In addition, they optimised the rolling strategy to minimise drag for a steady roll manoeuvre. Seigler et al. [9] investigated asymmetrical span extension for increased manoeuvrability of bank-to-turn cruise missiles. By formulating a full nonlinear model of the missile, due to the shift of the missile centre of mass and the dependence of the rolling moment on the angle of attack, they showed that the control authority can be significantly larger when compared to conventional tail surface control. Improved manoeuvrability, however, is highly dependent upon the angle of attack, linear actuation speed, and extension length. Moreover, as the mass of the extending wings becomes large relative to the missile body, the rigid body dynamics can become increasingly complex and a nonlinear control law was formulated to control the roll, angle of attack, and side slip angle dynamics in accordance with bank-to-turn guidance. The control method proved to be adept in tracking commanded inputs while effectively eliminating sideslip. A more extensive review on span morphing technology (applications and concepts) for both fixed-wing and rotary-wing aircraft is given in Barbarino et al. [10].

The main objective of this paper is to develop a structural concept that allows the wing span to be varied to provide roll control and enhance the operational performance of a MALE UAV. Equivalent modelling of the concept is performed using Euler-Bernoulli beam theory and thin-walled structures. Then preliminary sizing, weight estimation, and sensitivity study are conducted to determine the feasibility and highlight the potential benefits and possible drawbacks.

II. Aerodynamics

The Tornado Vortex Lattice Method (VLM) was used for aerodynamic predictions. Tornado is a linear aerodynamics code, and thus it discounts wing thickness and viscous effects [11]. These limitations imply that Tornado can only be used for angles of attack up to 8-10° for slender wings. Linear aerodynamic theory is still nevertheless very useful as most aircraft typically operate within the linear region (operating lift coefficients at reference speeds) in cruise/endurance, as well as both take-off and landing phases. These are the flight stages in which most of this research and analysis has been undertaken. In Tornado, usually one half of the wing is built and then mirrored with respect to the centerline of the aircraft to generate the entire wing. In order to investigate roll control using span morphing, each half of the wing is built separately to allow the asymmetric change in span. Typically the wing is defined from the root to the tip in Tornado for the symmetric case. However for the asymmetric case, one half of the wing is defined from root to tip and the other half is defined from tip to root. As the wing semi-span starts to increase the size of the spanwise elements start to increase resulting in a coarser aerodynamic mesh. A convergence study was performed to determine the size of the aerodynamic mesh required to generate accurate and robust results. Five chordwise elements and 20 spanwise elements are sufficient to provide robust prediction with a relative error of 0.05%. A linear distribution for the spanwise and chordwise panels was adopted.

A MALE UAV similar to the BAE Systems Herti UAV [12] (shown in Fig. 1a) was selected for this study. The UAV is modelled in Tornado VLM as shown in Fig. 1b and has a maximum lift to drag ratio of about 20 and a maximum endurance capability of about 18 hours. Figure 1b also shows the position of the Mean Aerodynamic Chord (MAC). A representative flight profile, shown in Fig. 2, was assumed in this analysis. The UAV takes-off with a weight of 800kg and it cruises and loiters for about 18 hours with a speed of 50m/s (M0.16) at 6100m (20,000ft) and then it descends and lands. The design parameters of the vehicle are given in Table 1.

a) BAE Systems Herti UAV [12]

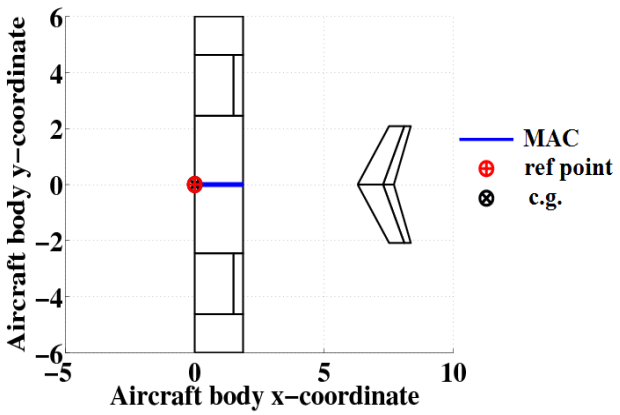

b) The MALE UAV in Tornado

Figure 1. The MALE UAV considered.

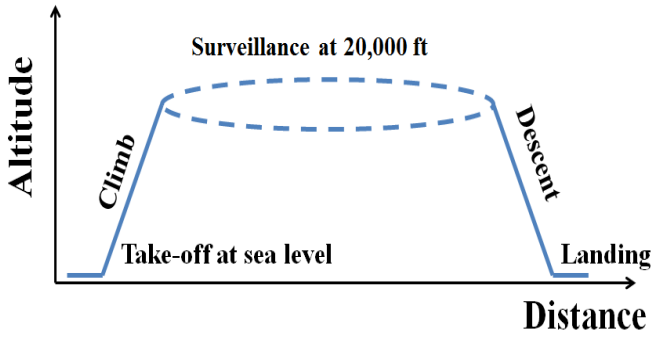

Figure 2. Mission profile of the UAV.

Table 1: Design parameters of the UAV

Design Parameters	Values
MTOW	800 kg
BOW	500 kg
Fuel weight	150 kg
Endurance	18 hrs.
Lift-to-Drag	20
Aerofoil	NACA 63-015A
Span	12 m
Chord	1.87 m
Wing area	22.44 m^2

MTOW: Maximum take-off weight
BOW: Basic operating weight

III. Benefits of Span Morphing

Ajaj et al. [13] investigated the use of asymmetric span morphing to provide roll control and replace conventional ailerons and assessed the potential benefits of symmetric span morphing in reducing vortex induced drag, extending endurance, and reducing take-off field length (TOFL) and landing distance (LD). The outcomes of their study can be summarised as

- The wing must be able to extend on both sides by up to 22% and must be able to retract on both sides by up to 22% to provide sufficient roll control over the entire flight profile.
- The rolling moment generated by asymmetric span morphing is very sensitive to the angle of attack (AOA). This sensitivity to AOA doesn't exist with conventional ailerons. This proves that morphing structures should not be operated in the same way as conventional control surfaces. The benefits that can be achieved from coupled manoeuvres must be exploited via the design of "ad hoc" flight control systems.
- Span morphing induces some additional inertial terms in the roll equation of motion. These increase the importance of the transient response compared to ailerons due to the larger and heavier structure to be actuated.
- 6% increase in flight endurance can be achieved with 22% symmetric span extension as shown in Fig. 3a.
- Finally, the wing designed to extend and retract up to 22% can achieve a 28% reduction in TOFL and a 10% reduction in LD as shown in Fig.3b.

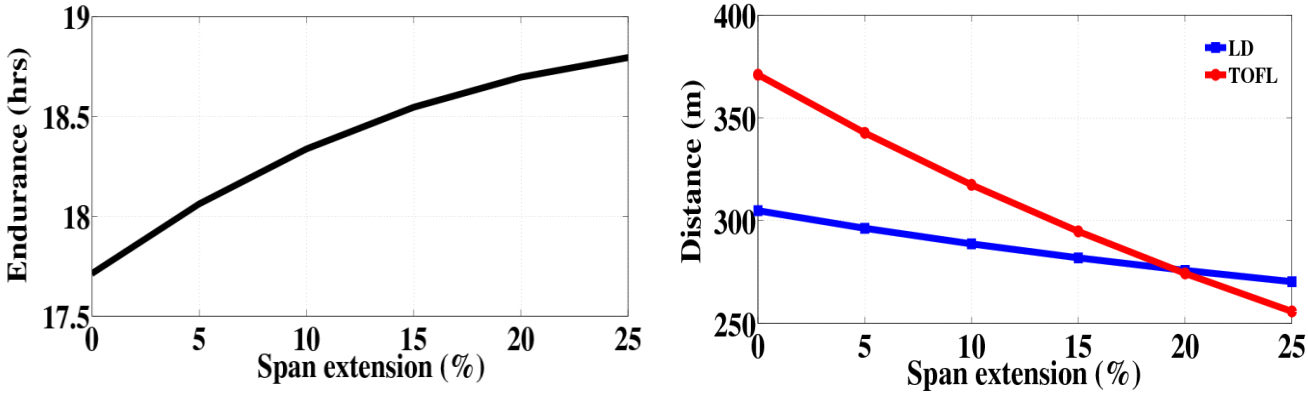

a) Change of endurance with span extension at different BOW

b) Variation of TOFL and LD with span extension

Figure 3. Operational performance benefits of Span morphing.

The ultimate benefits of the span morphing technology reduce as the Basic Operating Weight (BOW) increases. The variation of endurance with BOW at 22% symmetric span extension is show in Fig. 4.

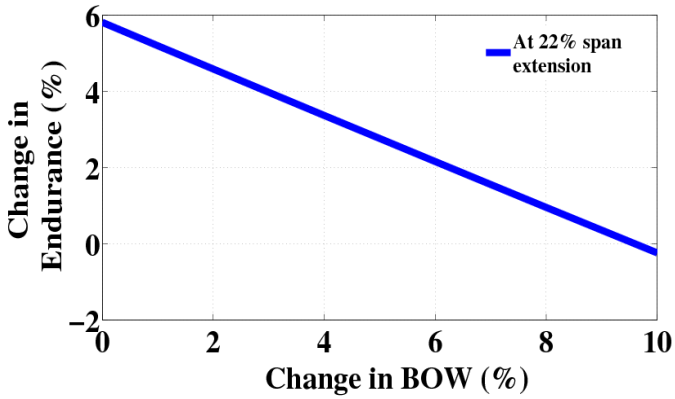

Figure 4. The change of Endurance with the BOW.

It should be noted that the variation of endurance with BOW is not linear but in the region up to 10% increase in BOW, it can be approximated as linear. The potential increase in endurance that can be achieved with 22% symmetric span extension reduces as the BOW increases and in fact the endurance can even go lower than that of the baseline UAV if the BOW of the morphing vehicle exceeds that of the baseline vehicle by more than 9.5%. This implies that the span morphing system (structure and actuator) must be as light as possible to maximise the gain in endurance. A variety of span morphing concepts can be found in the literature varying from telescopic structures with sliding skins actuated pneumatically or hydraulically to complaint structures with flexible skins actuated using SMA or muscles. However, only a limited number of vehicles with span morphing wings were built and flown. There are many reasons for this and they are beyond the scope of this paper. Table 2 summarises most of the aircraft that were built and flown with variable wing span or aspect ratio.

Table 2: Air-vehicles flew with span morphing technology

Vehicle	Category	Morphing	Structure	Skin	Actuator
MAK-10	GA	Span	Telescopic	Sliding	Pneumatic
MAK-123	GA	Span	Telescopic	Sliding	Pneumatic
FS-20	Glider	Span	Telescopic	Sliding	Screw jacks
FLYRT	UAV	Span	-	-	-
Virginia Tech	UAV	Span	Telescopic	Sliding	Rack and pinion
MFX-1	UAV	Aspect Ratio & Sweep	Articulated lattice structure	Stretchable	

Table 2 shows that most of the vehicles used telescopic structures where the morphing partition(s) can slide in and out through the fixed inboard partition. These vehicles do not require any complaint or flexible skin, as the sliding/telescopic mechanism allows rigid covers and semi-monocoque construction. In order to move away from conventional telescopic mechanisms, the Zigzag wingbox concept is developed and discussed here. In this paper a detailed preliminary analysis is performed to assess the feasibility of the concept. This kind of analysis is rarely found in literature and the lack of such studies is one of the main drawbacks with the research related to morphing aircraft.

The Zigzag wingbox as shown in Fig. 5 consists of two main parts, the rigid (non-morphing) wingbox and the Zigzag wingbox (morphing part). The rigid wingbox which is located near the wing root is a semi-monocoque construction similar to that of the baseline wing of the UAV consisting of two straight spars running spanwise with stressed covers (skin and stringers) and ribs running chordwise. The rigid wingbox houses the fuel tank and transfers the loads of the Zigzag wingbox to the fuselage. The Zigzag wingbox consists of various morphing partitions and each partition consists of two spars located at the leading and trailing edge respectively. Each spar consists of two hinged C-beams. The angle between those two beams can be varied during actuation which increases the effective span of the morphing elements. The rotation of the beams in each morphing partition with respect to the centreline of the wing allows the span or length of the partition to be altered (extending or retracting depending on the rotation). Each spar is also hinged at its two ends and attached to the adjacent ribs.

In addition, the ribs transfer the loads from the spars of one partition to the adjacent one until the load is transferred to the inboard rigid part which then transfers the loads through the bulkheads to the fuselage. In addition, to avoid local deformation of the flexible skins, the skins are only connected to the ribs and not to the spars. The use of flexible skins capable of large in-plane strain implies that the Zigzag wingbox (spars and ribs) must carry all the aerodynamic loads as the flexible skin can no longer withstand the large aerodynamic loads and their main role is to maintain a smooth aerodynamic shape and transfer the aerodynamic loads to the ribs and then to the spars.

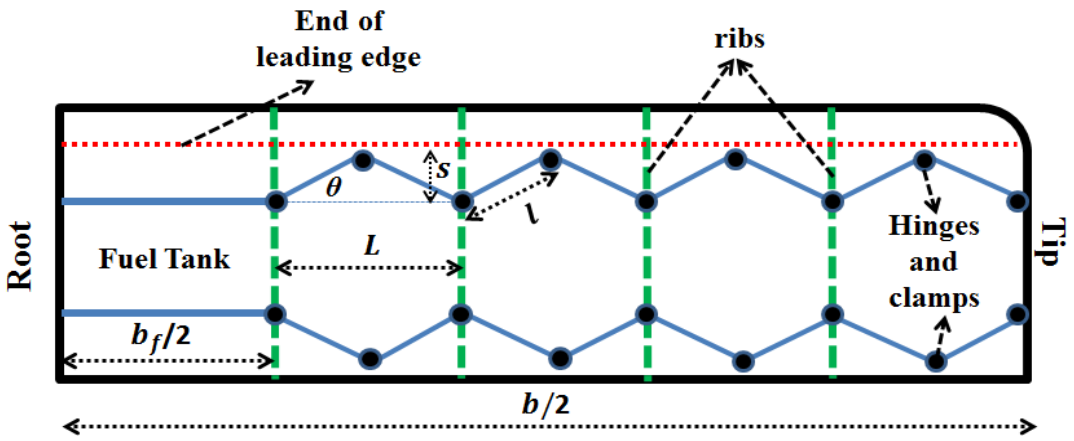

Figure 5. Top-view of the Zigzag wingbox concept.

A) Fuel Tank Span

The UAV wing must carry up to 150 kg of aviation gasoline to perform its mission. The fuel tank must be sized to carry the mission fuel as well as a 6% allowance for reserve and trapped fuel [14]. The aviation gasoline has a density of 0.72kg/l [14]. This implies that a fuel volume of 0.2208 m^3 is required. The rigid part has the front spar located at 20% of the chord and the rear spar at 65% of the chord. This means that the width of the fuel tank is about 0.84 m. The NACA 63-015A aerofoil has a maximum depth of 0.28 m. Assuming that the fuel tank depth is 80% of the maximum depth, the fuel tank span (b_f) can be estimated as 1.20 m. This means that the span of the rigid part of the Zigzag wingbox is almost 1.20 m.

B) Kinematics

The number of morphing partitions (n_p), the length of each C-beam (l), and the angle (θ) for any morphing condition can be obtained from geometry. By examining Fig. 5, l can be expressed as

$$l = \frac{s}{sin\theta_r} \tag{1}$$

where s is the distance from the end leading edge to the front spar when fully extended $(\theta = 0)$ and θ_r is the angle when the wing is fully retracted. For the morphing part, the front spar is located at 20% of the chord and the rear spar is located at 65% of the chord and the width of the leading edge is 10% of the chord. Therefore, s is 10% the chord which is equal to 0.187 m. Similarly, from geometry, the following correlations can be determined:

- When the wing is fully retracted:

$$2l\ cos\theta_r n_p = \frac{b_r - b_f}{2} \tag{2}$$

- When the wing is unmorphed:

$$2l\ cos\theta_b n_p = \frac{b - b_f}{2} \tag{3}$$

- When the wing is fully extended:

$$2l\ n_p = \frac{b_e - b_f}{2} \tag{4}$$

where b_r is the span of the wing when fully retracted, b_e is the span of the wing when fully extended, and b is the span of the baseline wing (12m). Using the equations above, θ_r and θ_b can be expressed as

$$\theta_r = cos^{-1}\left(\frac{b_r - b_f}{b_e - b_f}\right) \tag{5}$$

$$\theta_b = cos^{-1}\left(\frac{b - b_f}{b_e - b_f}\right) \tag{6}$$

It should be noted that θ_r and θ_b are independent of n_p and l as they represent relative changes in the partition length regardless of the length of the partition. Once θ_r is obtained, n_p and l can be computed from Equations (1) and (2). The design parameters of the Zigzag wingbox are listed in Table 3.

Table 3: Design parameters of the Zigzag wingbox

Parameter	Value
Theta at full retraction (θ_r)	54
Theta at base span (θ_b)	37
Number of morphing partition (n_p)	15
Length of truss (l)	0.23

C) Equivalent modelling

For such a concept to be feasible, it must be light and have a sufficient structural rigidity to withstand ultimate loads and have minimal vibration and large flutter margin. The first step to assess the feasibility of the concept is to perform preliminary sizing and weight estimation. Each spar consists of two beams hinged together and each spar is hinged at its ends to the adjacent ribs.

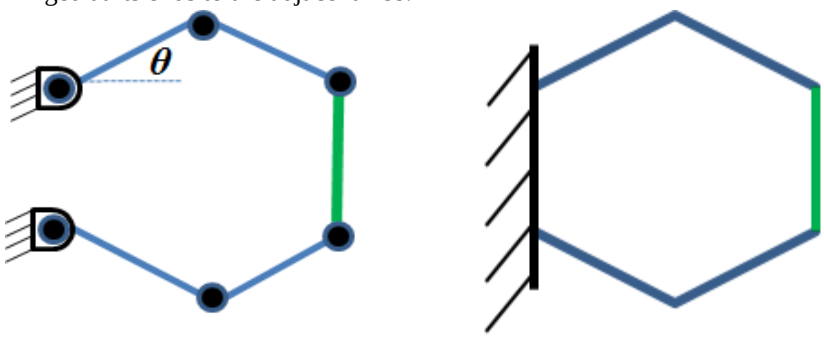

a) Actual arrangement b) Idealised arrangement

Figure 6. Actual versus Idealised arrangment of the Zigzag wingbox in a morphing partition.

The mechanism in Fig.6a which represents one morphing partition has 3 degrees of freedom and therefore three locking mechanisms are required for each morphing partition. Even if the mechanism is locked (cannot move as a rigid body), this does not necessary imply a continuous transfer of moments. For continuous transfer of moments, each hinge must have a locking mechanism (clamp) or the effective strength and stiffness of the arrangement drops. The clamp at each hinge allows the above mechanism to be modelled as a continuous structure clamped at one end and free at the other as shown in Fig.6b. The idealised arrangement in Fig.6b allows the axial, spanwise bending, chordwise bending, and torsional stiffness of the partition to be computed.

Due to symmetry it is sufficient to consider only half of the geometry of the morphing partition as shown in Fig.7. Then the resultant stiffness of the spar AC can be doubled to obtain the equivalent stiffness of the morphing partition. Consider the continuous spar AC which is clamped at A and free at C. Beam AB is at angle θ with respect to the wing X-axis while beam BC is at angle $-\theta$. Therefore, the Euler-Bernoulli's stiffness matrix of beam AB is obtained then is transformed from its local coordinates to the wing coordinates and similar process is performed for BC. Six degrees of freedom are considered for each node.

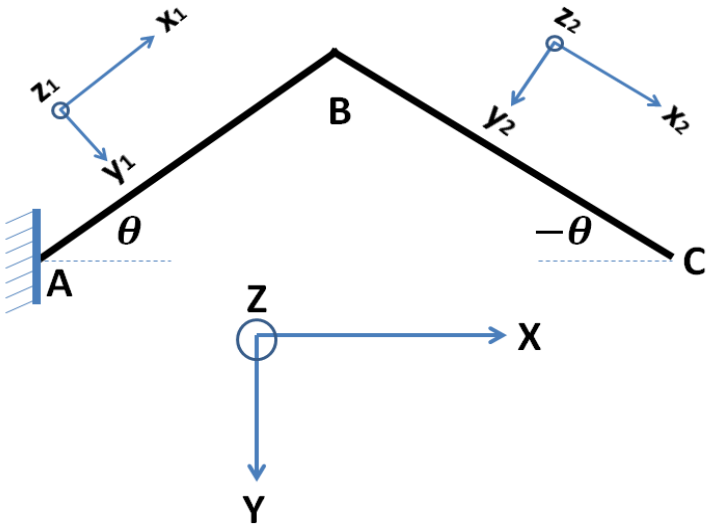

Figure 7. Idealised Spar model.

Then the global stiffness matrix of spar AC is assembled. This results in an 18x18 stiffness matrix. Due to the clamped boundary condition at A, the matrix can be reduced to become a 12x12 matrix. In order to obtain the equivalent axial stiffness of spar AC a unit force in the X-direction is applied at point C. This induces an axial displacement (along X-axis), a bending displacement (along Y-axis), and bending rotation (around Z-axis) at B. A boundary condition is applied at Point C to allow displacement only the X-direction. The axial stiffness of spar AC can be expressed as

$$K_x = \frac{a_1 b_1}{2(b_1 cos^2\theta + a_1 sin^2\theta)} \tag{7}$$

Terms $a_1$and b_1 are defined in Table 4. Thus, the equivalent axial stiffness of the morphing partition can be deduced as

$$K_{x_{eq}} = 2K_x = \frac{EA_{eq}}{L} \tag{8}$$

where L the length of a morphing partition and can be expressed as

$$L = 2lcos\theta \tag{9}$$

E is the Young's modulus and A_{eq} is the equivalent area of the partition. Rearranging Equation (8), A_{eq} can be expressed as

$$A_{eq} = \frac{24AI_z cos\theta}{12I_z cos^2\theta + Al^2 sin^2\theta} \tag{10}$$

where A is the cross-sectional area of the C-beam and I_z is the second moment of inertia of the C-beam around z_1. In order to obtain the equivalent spanwise bending stiffness of spar AC, a unit force in the Z-direction is applied at point C. This induces bending displacement (along Z-axis), bending rotation (around Y-axis) and twist (around X-axis) at B. A boundary condition is applied at Point C to allow only displacement in the Z-direction. The spanwise bending stiffness of beam AC can be expressed as

$$K_z = \frac{(c_1c_3 - c_2^2)cos^2\theta + c_1d_1sin^2\theta}{2(c_3cos^2\theta + d_1sin^2\theta)} \tag{11}$$

Terms c_1, c_2, c_3, and d_1 are defined in Table 4. Thus, the equivalent bending stiffness of the morphing partition can be deduced as

$$K_{z_{eq}} = 2K_z = \frac{12EI_{y_{eq}}}{L^3} \tag{12}$$

Rearranging Equation (12), the equivalent inertia $\left(I_{y_{eq}}\right)$ can be expressed as

$$I_{y_{eq}} = \frac{8I_ycos^3\theta\left(EI_ycos^2\theta + GJsin^2\theta\right)}{4EI_ycos^2\theta + GJsin^2\theta} \tag{13}$$

where G is the shear modulus, I_y is the second moment of inertia of the C-beam around y_1, and J is the torsion constant of the C-beam. Similarly to obtain the chordwise bending stiffness of spar AC, a unit force in the Y-direction is applied at point C. This induces a bending displacement (along Y-axis), bending rotation (around Z-axis), and an axial displacement (along X-axis) at B. A boundary condition is applied at Point C to allow only displacement in the Y-direction.

$$K_y = \frac{a_1(b_1b_3 - b_2^2)}{2(a_1b_3cos^2\theta + (b_1b_3 - b_2^2)sin^2\theta)} \tag{14}$$

Terms b_2 and b_3 are defined in Table 4. Thus, the equivalent bending stiffness of the morphing partition can be deduced as

$$K_{y_{eq}} = 2K_y = \frac{12EI_{z_{eq}}}{L^3} \tag{15}$$

Rearranging Equation (15), the equivalent inertia $\left(I_{z_{eq}}\right)$ can be expressed as

$$I_{z_{eq}} = \frac{2AI_zl^2cos^3\theta}{Al^2cos^2\theta + 3I_zsin^2\theta} \tag{16}$$

The torsional stiffness (K_θ) of spar AC can be obtained by applying a unit torque around the X-axis at point C. This induces a spanwise bending displacement (along Z-axis) and rotation (around Y-axis) at point B. A boundary condition is applied at Point C to allow only rotation around the X-axis. The equivalent torsional constant of spar AC (J_s) can be obtained by rearranging the expression of K_θ as

$$J_s = L\frac{K_\theta}{G} \tag{17}$$

In fact, the expression of K_θ is complex and therefore it is not included in the body of the paper. In contrast to the axial, spanwise bending, and chordwise bending cases, the torsional stiffness of the morphing partition is not just double that of spar AC. This is because K_θ is the torsional stiffness of spar AC around its axis and therefore to find the equivalent torsional stiffness of the morphing partition, it is necessary to transfer the rotation from the spar axis of rotation to the partition rotational axis as shown in Fig.8a. The morphing partition can be modelled as shown in Fig. 8b.

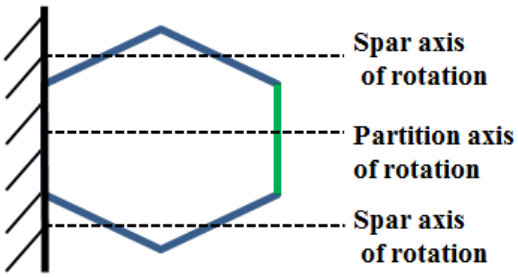

a) Rotational axes in the Zigzag wingbox

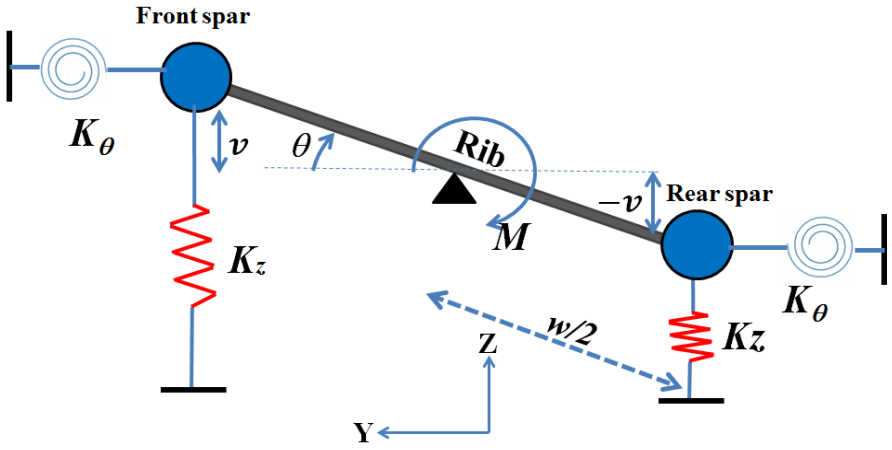

b) 2D Equivalent model of the morphing partition

Figure 8. Modelling of the equivalent torsional stiffness of a morphing partition.

The total potential elastic energy of the arrangement in Fig.8b can be expressed as

$$U = 2\left(\frac{1}{2}K_\theta\theta^2 + \frac{1}{2}K_y v^2\right) \tag{18}$$

where v is the vertical displacement at the spar end due to spanwise bending. Assuming small angles, from geometry v can be related to θ as

$$v = \frac{w}{2}\theta \tag{19}$$

The partial derivative of the potential energy with respect to θ represents the elastic restoring moment of the system once an external moment is applied

$$\frac{\partial U}{\partial \theta} = 2\left(K_\theta + K_y\frac{w^2}{4}\right)\theta \tag{20}$$

To obtain an expression for the equivalent torsion constant of the morphing partition, consider applying a torque (M) around the rotational axis of the partition. This torque can be expressed as

$$M = \frac{GJ_{eq}}{L}\theta \tag{21}$$

where J_{eq} is the equivalent torsion constant of the morphing partition. For static equilibrium to be established, the internal elastic moment must balance out the external torque. This allows J_{eq} to be expressed as

$$J_{eq} = \frac{2L}{G}\left(K_\theta + K_y\left(\frac{w}{2}\right)^2\right) \tag{22}$$

Table 4: Definition of stiffness terms

Term	Equation	Term	Equation
a_1	$\frac{EA}{l}$	c_1	$12\frac{EI_y}{l^3}$
b_1	$12\frac{EI_z}{l^3}$	c_2	$6\frac{EI_y}{l^2}$
b_2	$6\frac{EI_z}{l^2}$	c_3	$4\frac{EI_y}{l}$
b_3	$4\frac{EI_z}{l}$	d_1	$\frac{GJ}{l}$

D) Sizing and weight estimation

The sizing of the wingbox must be performed at the critical flight condition. This occurs at the start of loiter where the instantaneous gross weight is 790 kg and the airspeed is the 50 m/s at 20,000 ft. Usually, MALE and HALE UAV are designed according to gust load factor. Using the FAR regulations Part 23, Section 23.341, the gust load factor for this UAV at the critical flight condition is estimated to be 6g for an upward vertical gust and -4g for a downward vertical gust. After identifying the load factors at the critical flight condition, three loading cases are considered for sizing the wingbox. These are shown in Fig.9. The first case is when the wing is fully retracted (-22%), the second when the wing span is equal to the baseline wingspan, and the third case is when the morphing is full extended (22%).

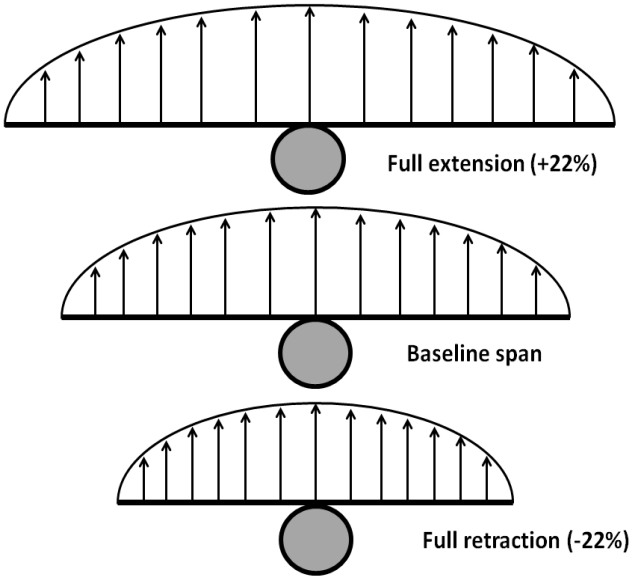

Figure 9. The three sizing cases.

The full extension flight scenario might seem the critical sizing case as the aerodynamic loads (bending moment and shear loads) increases significantly. However, this might not be true as the structure has its maximum stiffness when fully extended and its minimum stiffness when fully retracted. This argument justifies considering the three flight scenario and not just the full extension one. For each of the cases shown in Fig. 9, the wing is discretised into elements of equal length and sizing of each element is performed. For each element the material thicknesses required to resist bending and shear are estimated. Each element is sized so that structural failure (strength and stiffness) must not occur unless ultimate loads are exceeded. Although some references suggest using a lower factor of safety (FS) for unmanned air systems, in this analysis a FS of 1.5 was adopted. In addition to sizing the Zigzag wingbox, the baseline wingbox of the UAV is sized, to compare their relative weight and assess the potential benefits of the Zigzag wingbox in maximising the endurance

benefits for a given amount of fuel. Table 5 summarises the material systems for each wingbox (conventional and Zigzag).

Table 5: Material systems of the primary wing structures

Wing	Component	Material
Baseline	Wingbox and ribs	Aluminium 2024-T3
Morphing	Wingbox fixed part	Aluminium 2024-T3
	Wingbox morphing part	
	Ribs	
	Skins for morphing part	Fibre reinforced elastomers

For the Zigzag wingbox, the spar flanges resists all the bending loads while the spar webs resist all the shear loads [15]. The flexible skins are not designed in this paper as their main function is to serve as a smooth aerodynamic surface and transfer the aerodynamic pressure to the ribs which then transfer the loads to the spars. The ribs are also designed here. Their webs are designed to withstand shear loads and must not buckle under shear. The rib flanges are designed to withstand the pitching moment and chordwise bending loads from drag. The thickness of the material required to resist bending stress for any partition can estimated from the following expression

$$\sigma = \frac{FS\, n_g\, BM\, h}{2I_{y_{eq}}} \leq \sigma^* \tag{23}$$

where n_g is the gust load factor, BM is the 1-g bending moment, $I_{y_{eq}}$ is the equivalent 2nd moment of inertia of the wing section, h is the effective depth of the wingbox, and σ^* is the ultimate tensile strength. Since the wing depth varies along the chord, an effective depth, h, was used. This effective depth (h) can be related to the maximum depth of the aerofoil, d_{max} , as

$$h = \eta_t d_{max} \tag{24}$$

where η_t is the bending efficiency factor and, according to Tornbeek [16], it can be assumed to be 80%. For the baseline wingbox (without morphing), $I_{y_{eq}}$can be easily related to the thickness of the bending material. However, for the Zigzag wingbox, it is not possible to have an explicit expression that directly links $I_{y_{eq}}$ to the thickness of the bending material. Therefore, the thickness of the bending material is obtained using an iterative process. Similarly the thickness of the material required to resist the shear loads at any partition can be obtained from the following expression

$$\tau = \frac{FS\, n_g Q_v}{A_w} \leq \tau^* \tag{25}$$

where Q_v is the 1-g shear force, A_w is the area of the material required to resist shear stress (the webs of the spars in this case), and τ^* is the ultimate shear strength of the material. It should be highlighted that the minimum gauge for materials thickness in both bending and shear is set to be 0.2 mm. The outcomes of the sizing process are summarised in Table 6.

Table 6: Weight breakdown of the primary wing structure

Wing	State	Wing span (m)	Structural component	Weight (kg)	Load factor (g)	Weight (kg)	Load factor (g)
Baseline	Baseline	12	Wingbox	22.3	-4/+6	22.3	-4/+6
			Ribs	11.4		11.4	
	Unmorphed	12	Wingbox	38	-4/+6	38	-4/+6
			Ribs	7.4		7.4	
Morphing	Full extension	14.6	Wingbox	31.7	-4/+6	35	-5/+7
			Ribs	7.6		8	
	Full retraction	9.4	Wingbox	51.4		44.3	-3/+5
			Ribs	7.3	-4/+6	6.8	

It should be highlighted that the load factor depends on the wing area, and due to span morphing, the wing area changes significantly when the wing is fully retracted or fully extended. Therefore using the same load factor for the three scenarios may results in over-designing the wing for the fully retracted case and under-designing the wingbox for fully extended. Table 6 shows the outcomes of sizing using the same load factor for the three scenarios and the outcomes when using the appropriate load factor for each scenario. This can have significant impact on the weight of the wingbox. By examining the weights in Table 6, it can be concluded that the full extension loading scenario is not the critical case for sizing the wing. To illustrate, let us consider the point 2 m from the wing root. When the wing is fully extended ($\theta = 0°$), the bending moment at this point is 3350 Nm. On the other hand, when the wing is full retracted ($\theta = 54°$), the bending moment at this point is 1945 Nm. The ratio of bending moments at this point is 1.70 between full extension and full retraction. Based on this, one expects that the full extension loading case to be the critical loading scenario. However, this can be true only if the bending rigidity remains the same at full extension and full retraction which is not the case. Figures 10 and 11 show the variation of moments of inertia for the spar and for the morphing partition at 2 m from the root.

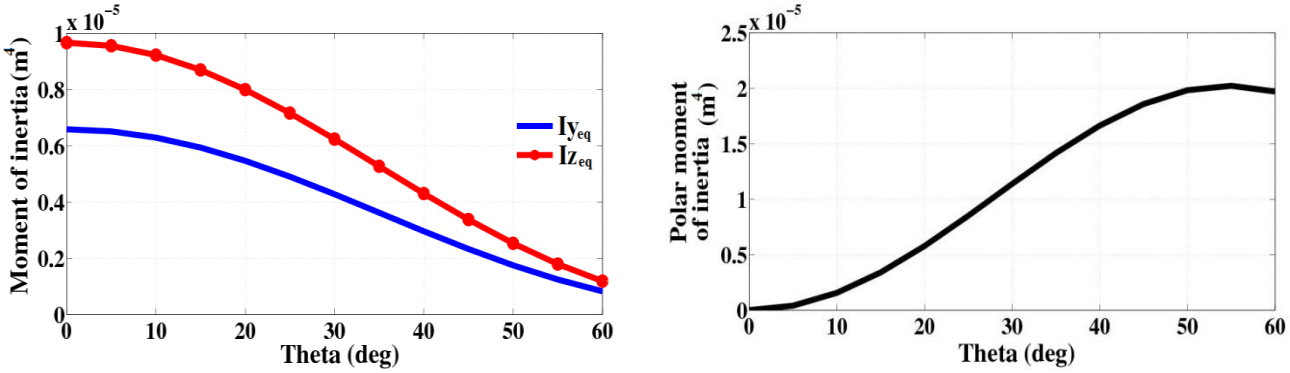

a) Variation of spanwise and chordwise moments of inertia of the spar

b) Variation of polar moment of inertia of the spar

Figure 10. Variation of moments of inertia of the spar with Theta at 2m from the wing root.

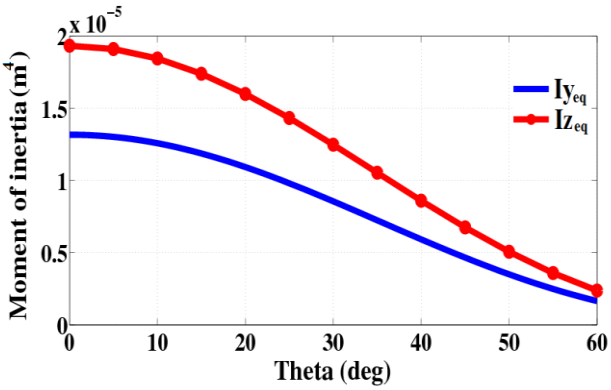

a) Variation of spanwise and chordwise moments of inertia of morphing partition

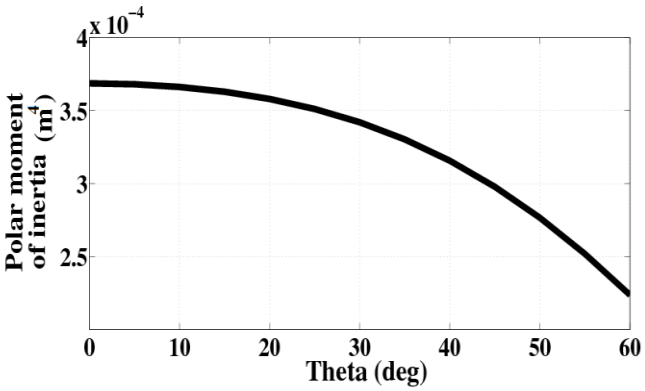

b) Variation of polar moment of inertia of the morphing partition

Figure 11. Variation of moments of inertia of morphing partitions with Theta at 2m from the wing root.

The ratio of $I_{y_{eq}}$ at fully extesnion to $I_{y_{eq}}$ at full retraction is about 5. This means that although the bending moment reduces by 70% at this location but the structural rigidity drops by five times. This justifies that the full retraction scenario is the most critical although it is associated with lower aerodynamic loads.

The spanwise bending stiffness of the wing has its maximum value when the wing is fully extended and has its lowest value when fully retracted. The wing is designed to withstand the ultimate gust load when fully extended and fully retracted. But if an active control system is used, then the wingbox weight can be significantly reduced. Since the Zigzag wingbox is very stiff when θ is zero (full extension), the role of the active control system is to fully extend the wing once the UAV is flying in a gust. The response of the control system must be very fast. If this is possible from a control and actuation points of view, then the structural weight of the wing can be reduced significantly. To illustrate, the wing when fully extended is sized to withstand up to -5/+7g with a FS of 1.5. On the other hand, the wing at full retraction and at baseline span must be sized to -1/+1g with a FS of 1.5. This allows saving about 9.3 kg in the wingbox weight. The outcomes of this analysis are summarised in Table 7.

Table 7: Zigzag wingbox weight with the Active Control System

Sizing case	Load factor (g)	Wingbox weight (kg)
Unmorphed	-1/+1	17.3
Full extension	-4.8/+6.8	35
Full retraction	-1/+1	18.4

E) Chordwise position of the spars

For a conventional wingbox, the chordwise position of the spars is not only determined by structural considerations but also by many factors including fuel tank size, leading and trailing edge surfaces, and landing gear position. However, since the morphing part of the Zigzag wingbox is not supposed to house the fuel tank or support any leading or trailing edge surfaces, the chordwise position of the spars can be altered. To understand the sensitivity of the wingbox weight to the spars position, the rear spar is fixed at 65% of the chord, and the position of the front web is altered gradually between 20% to 35% of the chord. However, it points out that the weight of the Zigzag wingbox is not affect by varying the position of the front spar in the morphing part of the wingbox. To illustrate, consider the cross-section of the C-beam shown in Fig.12.

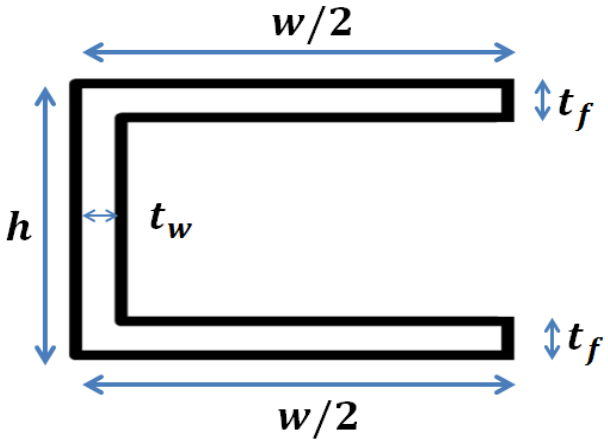

Figure 12. The cross-section of the C-beam.

The total weight of the Zigzag wingbox consists of two main components in addition to the weight of the hinges and their corresponding clamps. These two main components are the rigid part (W_r) and the morphing part (W_m)

$$W_Z = W_m + W_r \tag{26}$$

By varying the chordwise position of the front spar of the morphing part, the weight of the rigid part will not be affected. From geometry, W_m can be expressed as

$$W_m = 4l\rho n_p\left(t_f w + t_w h\right) \tag{27}$$

where t_f is the thickness of the flange, t_w is the thickness of the web, and ρ is the density of the material. *C*-beams tend to have a very low torsional constant (J) since they have open sections which make them fragile under torsional loads. This means that in Equation (13) the term $(GJsin^2\theta)$ is very small compared to $\left(EI_y cos^2\theta\right)$. This allows the equivalent spanwise bending stiffness expression of the morphing partition to be simplified as

$$I_{y_{eq}} \approx 2I_y cos^3\theta \tag{28}$$

Using the thin-walled approximation, I_y of the C-beam can be expressed as

$$I_y \approx \frac{1}{4} w t_f h^2 \tag{29}$$

Rearranging Equation (23), the area of the flanges of the C-beam can be expressed as

$$wt_f = \frac{4FS\ n_g M}{h\sigma^* cos^3\theta} \tag{30}$$

On the other hand, by rearranging Equation (25), t_w can be approximated as

$$t_w = \frac{FS\ n_g\ Q_v}{2h\tau^*} \tag{31}$$

$$t_w h = \frac{FS\, n_g\, Q_v}{2\tau^*} \tag{32}$$

This means that for a given θ, wt_f (area required to resist bending) and $t_w h$ (area required to resist shear) are constants. This means that the weight of the morphing part of the Zigzag wingbox does not vary with the chordwise position of the spars which implies that if the front spar is placed at 35% instead of 20% of the chord, l can be increased from 0.23 m to 0.56 m. This allows means the number of the morphing partitions to be reduced from 15 to 6 and thus lower number of hinges, clamps, and ribs are required. A model of the Zigzag wingbox concept was generated in AutoCAD 2010. Figure 13 shows the concept in top and isometric views.

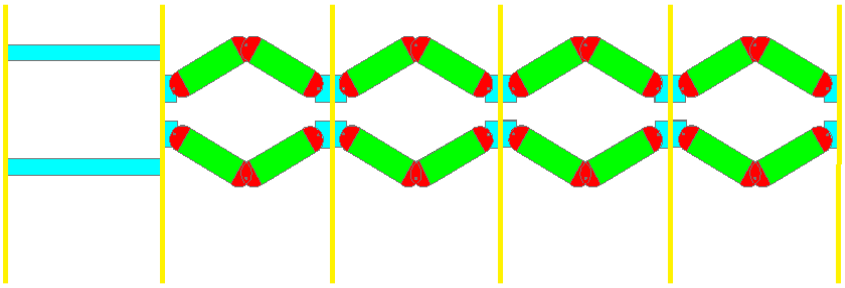

a) The Zigzag wingbox in top view

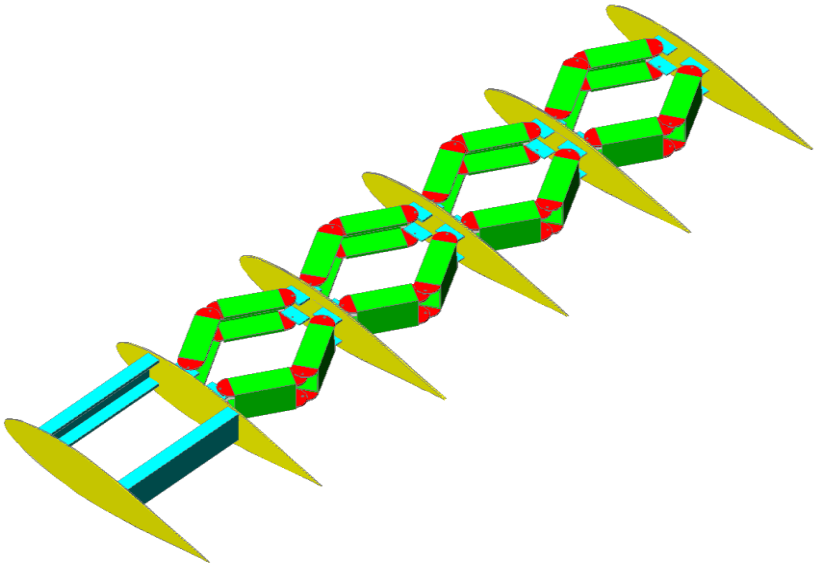

b) The Zigzag wingbox in isometric view

Figure 13. The Zigzag wingbox in AutoCAD 2010.

F) Quasi-static Aeroelasticity

After sizing of the wingbox to resist bending and shear loads, a quasi-static aeroelastic check is performed to ensure that the wing deformation under aerodynamic loads are minimal to avoid distorting the lift distribution which increases drag and reduces the endurance benefits of span morphing. The wingbox is modelled as a one dimensional linear Euler-Bernoulli beam. The beam is discretised into elements (synchronised with the discretisation for sizing) with each element having two nodes at its extremities. Each node has six degrees of freedom: three in translation and three in rotation. The stiffness matrix for each element is determined using the equivalent geometric and mechanical properties of the element. The loads (forces and moments) on each node

are then estimated using the Tornado VLM, and hence, the wing nodal deflections can be estimated. The quasi-static aeroelastic check requires an iterative solution to estimate the wing deformations, while accounting for the strong interaction between the aerodynamics and the structure. The iterative solution continues until equilibrium between aerodynamic loads and structural deformations is achieved. If equilibrium is not achieved than the material thickness for bending and shear has to be increased until equilibrium is achieved. Figure 14 shows the aeroelastic deformation of the wing when fully extended.

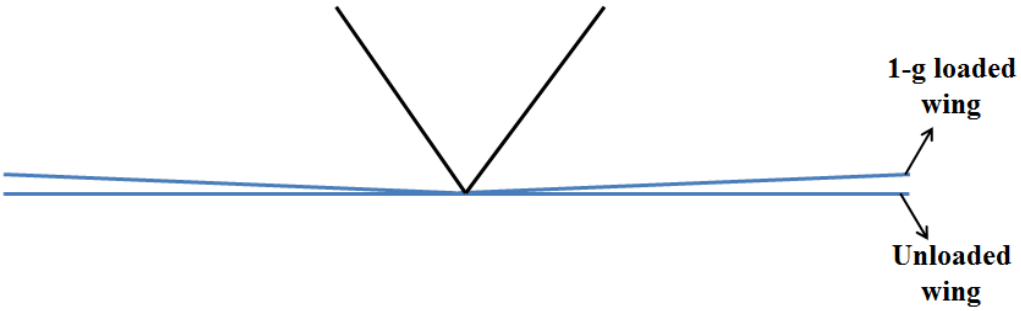

Figure 14. Aeroelastic deformation of the wing when fully extended.

G) Practicality and feasibility

As stressed above, the gain in endurance reduces as the structural weight of the Zigzag wingbox increase. Table 8 summarise the gain in endurance with the Zigzag wingbox for the case where there is no control system and for the case where there is an active control system.

Table 8: Gain in endurance with the Zigzag wingbox

Zigzag wingbox and ribs weight (kg)	Change in BOW (%)	Gain in endurance (%)
44.3	+3.5	+3.7
35 (with control system)	+ 1.9	+4.7

The main practicality issue with the Zigzag wingbox is that during actuation, the wingbox can still carry the loads due to lift, but as the hinges are not flexible, the wingbox can undergo sweep passively due to the drag force. This is a passive and unwanted mode of deformation that can jeopardise the benefits of the concept and therefore, the actuator must be able to withstand these loads during actuation and prevent passive sweep which might increase the weight and complexity of the actuation system.

IV. Conclusion

The Zigzag wingbox is shown to be a promising concept capable of delivering the variation in wing span required. However, its weight is almost double the weight of the conventional wingbox. In addition, the Zigzag wingbox is associated with structural complexity due to the need for hinges and locking mechanisms required to maintain structural integrity and at the same time allow large structural deformation. Although the Zigzag wingbox concept shows to be relatively heavy, still about 4% increase in endurance can be achieved for this MALE UAV. This 4% might drops when flexible skins and hinges are considered. Probably, the final benefit in endurance will be about 3% increase and about 4% if the active control system is considered.

The concept seems to be more feasible on smaller scale UAVs where lower number of morphing partitions and smaller structural deformation are required. The equivalent modelling performed here highlights the importance of simple low fidelity tools to assess the benefits of morphing structures due to the large design space available.

The kind of detailed analysis performed in this paper is rarely conducted for most morphing concepts available in literature. A morphing concept must not only allow shape change but also must be more efficient

from structural and actuation points of view when compared to conventional structures. The benefits of the Zigzag wingbox concept can be more exploited by considering the coupling between sweep and span. On major difficulty with complaint morphing concept (such as the Zigzag wingbox) is that the skins have to be flexible to allow structural deformations and thus they cannot withstand large aerodynamic loads, they just serve as a smooth aerodynamic surface. This prevents complaint morphing concepts from having the structural benefits of semi-monocoque construction and requires overdesigning their internal structure (spars and ribs) to withstand the loads.

Acknowledgments

The research leading to these results has received funding from the European Research Council under the European Union's Seventh Framework Programme (FP/2007-2013) / ERC Grant Agreement n. [247045]. The first author acknowledges support and feedback from the Visionary Aircraft Concept (VAC) Group at Bauhaus Luftfahrt e.V., Munich, Germany.

References

1. McCormik, B.W. *Aerodynamics, Aeronautics and Flight Mechanics*, 2nd Edition, Wiley, New York, 1995.
2. Weisshaar, T.A. "Morphing Aircraft Technology – New Shapes for Aircraft Design," RTO-MP-AVT-141, Neuilly-sur-Seine, France, 2006.
3. Blondeau J. and Pines D. "Design and Testing of a Pneumatic Telescopic wing for Unmanned Aerial Vehicles," AIAA, Journal of Aircraft, 44(4), 2007.
4. Blondeau J., Richeson, J. and Pines D.J. "Design, Development and Testing of a Morphing Aspect Ratio Wing Using an Inflatable Telescopic Spar," 44th AIAA/ASME/ASCE/AHS/ASC Structures, Structural Dynamics and Materials Conference, Norfolk, VA, AIAA 2003-1718, 2003.
5. Ivanco, T.G., Scott, R.C., Love, M.H., Zink, S. and Weisshaar, T.A., "Validation of the Lockheed Martin Morphing Concept with Wind Tunnel Testing," 48th AIAA/ASME/ASCE/AHS/ASC Structures, Structural Dynamics, and Materials Conference, Honolulu, Hawaii, AIAA 2007-2235, 2007.
6. Bye, D.R. and McClure, P.D. ''Design of a Morphing Vehicle,'' 48th AIAA/ASME/ASCE/AHS/ASC Structures, Structural Dynamics, and Materials Conference, 23-26 April, Honolulu, HI, AIAA 2007-1728, 2007.
7. Love, M.H., Zink, P.S., Stroud, R.L., Bye, D.R., Rizk, S. and White, D. "Demonstration of Morphing Technology through Ground and Wind Tunnel Tests," 48th AIAA/ASME/ASCE/AHS/ASC Structures, Structural Dynamics, and Materials Conference, Honolulu, Hawaii, AIAA 2007-1729, 2007.
8. Ajaj, R.M., Friswell, M.I., Saavedra-Flores, E.I., et al. "Span Morphing: A Conceptual Design Study," 20th AIAA/ASME/AHS *Adaptive Structures Conference*, 23-26 April 2012, Honolulu, Hawaii, USA, paper AIAA-2012-1510, 2012.
9. Seigler, T.M., Bae, J.S. and Inman, D.J. ''Flight Control of a Variable Span Cruise Missile,'' In: Proceedings of 2004 ASME International Mechanical Engineering Congress and Exposition, 13-19 November, Anaheim, CA, Paper No. IMECE2004-61961, 2004.
10. Barbarino, S., Bilgen, O., Ajaj, R.M., Friswell, M.I., and Inman, D.J., "*A Review of Morphing Aircraft*," Journal of Intelligent Material Systems and Structures, 22(9), 823-877, June 2011.
11. Melin, T. A Vortex Lattice MATLAB Implementation for Linear Aerodynamic Wing Applications. Master's Thesis, Royal Institute of Technology (KTH), Department of Aeronautics, Sweden, 2000.
12. BAE Systems Military Air Information, "HERTI Next Generation Autonomous System Factsheet", June 2011.
13. Ajaj, R.M., Friswell, M.I., Isikveren, A.T. Saavedra Flores, E.I., Allegri, G., and Dettmer, W.G. "Span Morphing Technology: An Integrated Conceptual Design Study," Journal of Intelligent Material Systems and Smart Structures, Submitted, August 2012.
14. Raymer, D.P. *Aircraft Design: A Conceptual Approach*, 4th Edition, AIAA, 2006.
15. Ajaj, R.M., Smith, D., Isikveren, A.T., and Friswell, M.I. "A Conceptual Wing-box Weight Estimation Model for Transport Aircraft," The Aeronautical Journal, 2012, Accepted.
16. Torenbeek, E. "Development and Application of a Comprehensive, Design-sensitive Weight Prediction Model for Wing Structures of Transport Category Aircraft," Report LR-693, Delft University of Technology, September 1992.